Resolution improvement techniques for microwave imaging in random media using small wideband adaptive arrays

Mark Curry*, Radar Signal Processing Group, Boeing Phantom Works
Yasuo Kuga**, Department of Electrical Engineering, University of Washington

ABSTRACT

In this work we review and extend the approach for radar imaging using small, wideband, adaptive arrays by using a ray-tracing algorithm to simulate non-homogeneous environments. This allows the rapid investigation of radar imaging in more realistic environments that might be encountered in practice. We have previously shown that such arrays can be effective for short range backscatter imaging and source localization in free space using experimental arrays of four elements at 1 GHz and 20% bandwidth as well as twelve elements operating from 2-3 GHz. These arrays have been constructed to test the proposed algorithms and have demonstrated good results. We review the spatial resampling technique for array focusing. We discuss Approximate Signal Subspace Projection (**ASSP**) to suppress clutter. This technique allows more control over the angular resolution and the background clutter level. We review the ray-tracing algorithm that is required to generate data for imaging. Computer simulations are shown to demonstrate the use of adaptive array imaging in several non-homogeneous environments. The motivations for this work are indoor personnel localization systems, automotive radar and radar imaging seekers.

Keywords: Radar imaging, wideband adaptive array

1. INTRODUCTION

Figure 1 shows the scenario for active microwave imaging. Alternately, the targets may consist of wideband signal sources. In either case, range resolution is achieved by wideband, stepped CW signals (FM-CW).

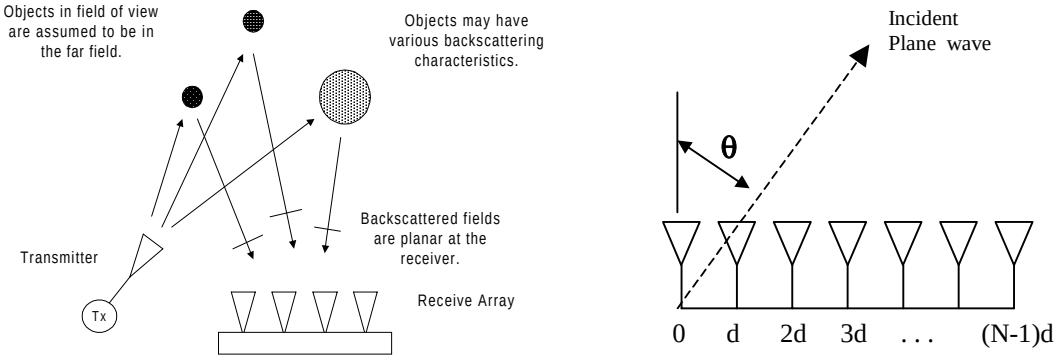

Fig. 1. Microwave Imaging Arrangement and Uniform Linear Array Geometry

In our previous work [1], [2], we discussed a four-channel array operating at about 1 GHz. These results were encouraging enough to construct a new system with twelve wideband elements operating at 2.5 GHz in free space [4] and [5], [19]. Reference [6] has reported results using a similar basic approach with an experimental adaptive array employing FM chirp in an outdoor environment but did not include the proper focusing for optimal angular resolution. In our work we have emphasized the need for proper compensation for dispersion so that imaging over a wide angular sector will be near optimal as well as the need to suppress clutter to improve resolution for small arrays. Our techniques

Advanced Signal Processing Algorithms, Architectures, and Implementations XII, Franklin T. Luk, Editor,
Proceedings of SPIE Vol. 4791 (2002) © 2002 SPIE · 0277-786X/02/$15.00

are in some ways a special case of superresolution SAR imaging [7], [8], [9], [10], however in this case the aperture consists of a small set of elements and images a wide angular sector. In addition, the clutter statistics will be different due to range-angle clutter distribution and the fact that in our case the angular resolution is constant, which results in a range-dependent crossrange resolution. The imaging approach utilizes adaptive beamforming techniques in crossrange only.

2. SIGNAL MODEL

First we briefly review the angular array geometry and the array outputs for wideband signals. Consider a superposition of fields backscattered from objects in the field of view of the transmitter. Assume objects are in the far field. The incident plane waves can be parameterized by their angle of arrival as shown in Fig. 1. For this FM-CW signal model, the baseband antenna output for frequency *m* and element *n*, for *Ntargs* scatterers at range r_i and angle θ_i is

$$V_o(n,m) = \sum_{i=1}^{i=Ntargs} \exp\left\{-j2\pi m\Delta f \frac{2r_i}{c_o}\right\} \exp\left\{-j2\pi \frac{f_o}{c_o} nd\sin\theta_i\right\} \exp\left\{-j2\pi\left(\frac{m}{M}-\frac{1}{2}\right)\frac{f_{BW}}{c_o} nd\sin\theta_i\right\} \quad (1)$$

Transmit frequency, $f_m = f_o + (m - M/2)\Delta f$ and f_o is the center frequency of the antenna. The first exponential term describes the phase information as a function of range, and the second and third terms describe the inter-element phase due to the incidence angle of the field. The second term describes the linear phase shift across the array for angle θ_i, which is independent of frequency. However the third term shows an additional phase across the array that is highly dependent on frequency $m\Delta f$. The affect of the last term is to cause the angle of arrival to appear to change as the incident field wavelength changes (dispersion). The angular variance is proportional to the true line-of-sight (LOS) angle. For large angles of arrival the angular broadening is greatest. The angular dispersion can be removed while not interfering with range phase information if the antenna phase center is held constant. A straightforward approach for "focussing" utilizes spatial resampling, [11] to map the incident fields to the narrowband plane wave model. Downrange resolution is a function of total bandwidth. A zero-padded FFT on each focused, array element output performs the pulse compression. Each range bin contains the superposition of target responses for all targets at the that range. Using a conventional (Fourier) approach for range compression allows for a minimum of target shape constraints in the range dimension. For example a target does not have to be point-like in the range dimension. This relaxes the model requirements somewhat. We use adaptive beamforming in the angle dimension to achieve improved resolution from a small antenna.

3. SPATIAL RESAMPLING AND IMAGE FORMATION

In this section we briefly review for completeness, the basic array focusing and image formation techniques that are needed to form a high quality image. The array outputs must be properly focussed so that the angle of arrival of a single plane wave is constant for a given temporal frequency. An adaptive signal processing view of this is that the signal model is low rank, i.e. parameterized by the angle of arrival only. One method for focusing, involves resampling the array outputs to correct for the constant element spacing d. See [11] for a discussion of spatial resampling techniques applied to wideband angle of arrival estimation for uncorrelated signals. For joint range-angle estimation we have the additional requirement that the antenna phase center for each resampled array output must remain fixed at the center of the array to preserve range information. As frequency m increases for a fixed spacing d, the angle of arrival appears to increase, so to offset this affect we extract samples closer to the center of an interpolated array. Conversely as the frequency decreases we must extract samples farther from the array center. This is analogous to changing the inter-element spacing as a function of frequency. The expression for the focused array output is derived by combining the 2nd and 3rd exponential terms from equation (1), set $\Delta f = f_{BW}/M$, and for center frequency f_o, the spacing is

$$d \quad = \quad d_o f_o \left(\frac{f_{\min}}{f_o} \right) \Big/ \left(f_o + \left(m - \frac{M}{2} \right) \Delta f \right) \tag{2}$$

where d_0 is the inter-element spacing. This value of d, focusses the array output into a superposition of narrowband plane waves at ranges r_i and angles θ_i.

$$V(m,n) = \sum_{i=1}^{i=Nt \arg s} \exp\left(-j2\pi m \Delta f \, 2\left(\frac{r_i}{c_o} \right) \right) \exp\left(-j2\pi \left(\frac{f_o}{c_o} \right) n d_o \left(\frac{f_{\min}}{f_o} \right) \sin\theta_i \right) \tag{3}$$

This result has the desired properties to employ narrowband adaptive beamforming techniques in an optimal way. We observe that the effective array spacing has been modified by $\beta = f_{\min} / f_o$ therefore the angular steering vectors are scaled by the same amount. This procedure will focus all targets at all ranges. Array focussing is performed in practice by interpolating between the known values at each element. In [11] an optimum in the least squares sense, resampling filter was developed to focus an incident field of known temporal frequency. We use a frequency-scaling factor to control the interpolation coefficients, which is proportional to frequency as defined by

$$h_m(n,k) = \frac{1}{\pi} \frac{\sin\{\Psi_m(\mu_m n - k)\}}{(\mu_m n - k)} \tag{4}$$

where we define

$$\mu_m = \frac{\beta f_0}{f_0 + (m - M/2)\Delta f} \qquad \text{and} \qquad \Psi_m = \min(\pi, \pi \frac{f_0 + (m - M/2)\Delta f}{\beta f_0})$$

and $\beta = f_{min} / f_o$. Next, we write the complete expression for interpolating the array data, *X(m,n)* for frequency *m* and element *n* to the focussed output *Y(m,n)* as

$$Y(m,n) = \sum_{k=0}^{N-1} h_m(n,k) X(m,k) \tag{5}$$

There is some flexibility in the choice of range Fourier transform size used for range compression. If the number of frequencies is a power of two then the range bins will be orthogonal to each other. This method has the minimum range sidelobes. However, to obtain a sufficient number of range samples may require significant processing time. In some cases this may be the preferred method. In other cases we may have a limited number of frequencies. In this case we can window the data, pad the data with zeros and then do a larger FFT size. This only interpolates the range dimension. The actual range dimension is a function of the total bandwidth. When using the zero-padded method there will be range sidelobes that show up as a scalloping in the range dimension only. We normally use the Hamming window since it is a good compromise between sidelobe suppression and resolution.

This section outlines the minimum variance spectral estimation method used to derive the angular spectrum at each range bin. The data from all bins at the same range are grouped together to form a vector $\mathbf{X}_m$, of *N* elements. This vector contains the angular information about all targets at the same range. Minimum variance spectral estimation is well known, and straightforward to implement [12]. Starting with the assumed steering vector $\mathbf{s}(\phi) = [e^{j0\phi}, e^{j1\phi}, \ldots, e^{j(N-1)\phi}]^T$, where $\phi = kd \sin\theta$, and θ is the angle of arrival of the incident plane wave. The received power at a particular steering angle is used to form the image and is given by

$$P(\phi) = \left(\mathbf{s}^H(\phi) \mathbf{R}^{-1} \mathbf{s}(\phi) \right)^{-1} \tag{6}$$

The spatial covariance matrix **R** is estimated from the average of outer products from independent and identically distributed (iid) samples of **x**, the observed data. For the case of image formation as discussed here, there are no iid samples for 2 reasons. The stationary scene has no Doppler information, and all targets at the same range, independent of angle, are correlated. It is however possible to combine multiple closely spaced groups of frequencies to mitigate the effects of white noise, such as thermal noise in the receiver. After computing the Fourier transforms of the element signals we usually have one single snapshot of data at each range bin from which to derive the angles of arrival of

objects at that range. For correlated signals and linear arrays, sub-array averaging (spatial smoothing) [13], [14], [15] is used to estimate a spatial correlation matrix from as little as one snapshot. After forward spatial smoothing, forward-backward averaging is used to significantly improve the estimate of **R**. The tradeoff for using spatial smoothing to estimate correlated signals is a smaller effective aperture, which leads to fewer degrees of freedom for beamforming. Additionally, the angular resolution is not as good as that obtained for uncorrelated signals.

One approach for improving the resolution involves squaring the correlation matrix **R,** before spatial smoothing. See [16] for a discussion of the method and the resolution properties of spatially smoothed correlation matrices. Squaring the correlation matrix increases the robustness of the dominant eigenvectors, which results in better resolution for closely spaced arrivals. This approach has been found to improve resolution over the spatially smoothed but non-squared approach. It provides consistent AOA estimates, but the variance of target RCS has been found to increase significantly and has a long-tailed distribution. In summary, the basic image formation procedure is as follows:

1. Capture S_{21} (backscattered) data over the frequency range required for range resolution.
2. Resample array data for each frequency to form the focussed data set.
3. Apply a FFT to the Hamming windowed, zero-padded data from each focussed element.
4. Pre-compute appropriate angular steering vectors from gain-phase calibration data (as required).
5. Estimate the spatial covariance matrix at each range bin by using sub-array averaging, forward-backward averaging and rank reduction filtering (**ASSP**). Add diagonal loading if required, if noise floor is very low.
6. Estimate the minimum variance (MV) angular spectrum at each range bin using sub-array averaging and forward-backward averaging to resolve correlated signals from targets at the same range.
7. Form the range angle image from the MV spectrum at each range bin.

Figure 2 shows simulated range-angle plots for a 12-element linear array operating from 2-3 GHz.

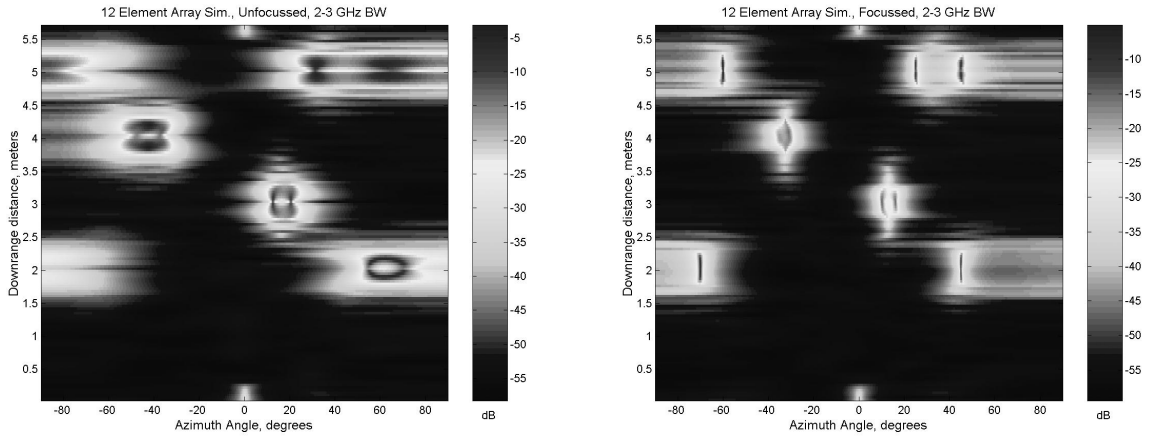

Fig. 2. Angular resolution comparison for simulated 12-element arrays, the left side is unfocussed and the right side is focussed. The two targets at 3m have 5° spacing, with 3 targets at 5m range.

4. APPROXIMATE SIGNAL SUBSPACE PROJECTION (ASSP)

In this section we review the derivation of **ASSP**. The radar background clutter will not in general, fit the low rank signal plus noise model that would like, i.e. the signal set consists of a superposition of plane waves. Diffuse clutter signals may easily span large angles. This has been readily observed in our electromagnetic test chamber. The backscatter from the chamber itself has a structure that is relatively strong and repeatable, due to constructive interference at the receive array from the integrated backscatter off of the cones which are radiated at oblique angles. The experimental 12-element imaging array is readily able to display the structure of this clutter. For targets such as dihedral reflectors about 2-3 wavelengths in size the background clutter is about 15-20 dB below the target return, but is

not really homogeneous across all ranges and angles of interest. The idea of **ASSP** is to increase the signal to clutter plus noise ratio (SCNR) by a rank reducing linear operator. We are concerned with the 'effective' rank' so the goal is to increase the robustness of the signal eigenvectors by attenuating the clutter and noise eigenvalues. In the case of correlated signals, if all other variables are held constant, then increasing the signal to noise ratio will improve the resolution. We start with the unitary decomposition of the signal covariance matrix. We assume the noise is white:

$$\mathbf{R} = \mathbf{U}_s \Lambda_s \mathbf{U}_s^H + \sigma^2 \mathbf{U}_s \mathbf{U}_s^H \tag{7}$$

The signal component will contain the signal and the clutter, with the clutter subspace associated with the smaller eigenvalues. We wish to estimate a lower effective-rank signal subspace to reduce the clutter contribution without doing an eigendecomposition and estimating the number of signals. While a full eigendecomposition and principal components estimation can be done in extremely high clutter levels, a similar net result can be approximated for low to medium clutter levels using the following linear operator **P:**

$$\mathbf{P} = \mathbf{R}^n (\mathbf{R}^n + \alpha^n \mathbf{I})^{-1} \tag{8}$$

If α>0, using the unitary decomposition $\mathbf{R} = \mathbf{U}\Lambda\mathbf{U}^H$ yields

$$\begin{aligned} \mathbf{P} &= (\mathbf{U}\Lambda\mathbf{U}^H)^n [(\mathbf{U}\Lambda\mathbf{U}^H)^n + \alpha^n \mathbf{I}]^{-1} \\ &= \mathbf{U}\Lambda^n \mathbf{U}^H [\mathbf{U}(\Lambda^n + \alpha^n \mathbf{I})\mathbf{U}^H]^{-1} \\ &= \mathbf{U}\Lambda^n (\Lambda^n + \alpha^n \mathbf{I})^{-1} \mathbf{U}^H \qquad \text{Define: } \mathbf{H}_s = \Lambda^n (\Lambda^n + \alpha^n \mathbf{I})^{-1} \\ &= \mathbf{U}\mathbf{H}_s \mathbf{U}^H \end{aligned} \tag{9}$$

Now multiply $\mathbf{R}$ and $\mathbf{P}$:

$$\boxed{\hat{\mathbf{R}} = \mathbf{P}\mathbf{R} = \mathbf{U}\mathbf{H}_s \mathbf{U}^H \mathbf{U}\Lambda\mathbf{U}^H = \mathbf{U}\mathbf{H}_s \Lambda \mathbf{U}^H}$$

Since Λ^n is diagonal, we may write down the expression for the diagonals of $\mathbf{H_s}$:

$$\mathbf{H}_s(i,i) = \frac{\lambda_i^n}{\lambda_i^n + \alpha^n} \qquad \begin{cases} \mathbf{H}_s(i,i) \to 1 & \text{for } \lambda >> \alpha \\ \mathbf{H}_s(i,i) \to 0 & \text{for } \lambda << \alpha \end{cases} \tag{10}$$

Figure 3 shows some eigenvalue transfer functions for choice of α and *n*. The higher that *n* is, the more rapid the transition. Values of *n* that have given good results are typically 2 to 4. Clearly the **P** matrix does not alter the eigenvectors of **R**, but acts as a highly linear cutoff function for eigenvalues of **R,** depending on their values relative to α. If the value of α is chosen properly then **P** will act as an approximate projector onto the eigenvectors of **R** with the largest associated eigenvalues.

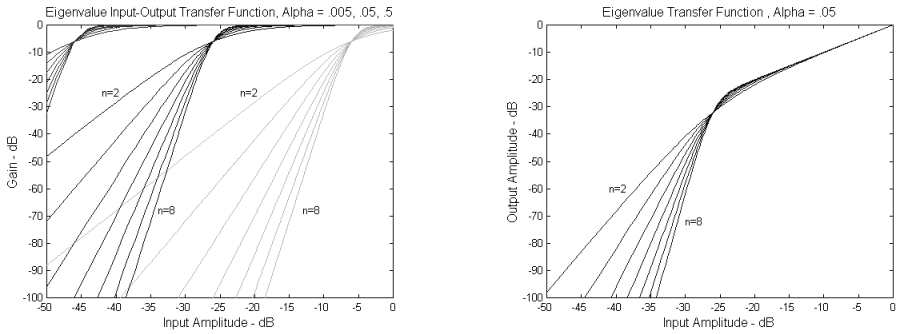

Fig. 3 Eigenvalue transfer functions as determined by *alpha*, *n*.

Effectively, matrix **P** will attenuate the eigenvectors of **R** with eigenvalues smaller than α. As an example, for *n*=2, to square the condition number of matrix **PR** set $\alpha = \sqrt{\lambda_{\max}\lambda_{\min}}$. This cutoff point is close to that of squaring the covariance matrix, but now there is control of the effective rank of the signal subspace, which allows for discrimination between target signals and background clutter. In order to estimate a value of α we must do a preliminary spectral estimate in order to find the peak signal level and the clutter and noise background level. As an example, consider the angular spectrum in Fig. 4 and the corresponding eigenvalue distribution. The data contains 3 strong signals, 2 of which are relatively closely spaced, and 1 signal at –20 dB relative to the other 3. In this case we have a peak signal to noise level of about 30 dB, with an associated peak eigenvalue to average noise eigenvalue level of about 30 dB. An estimate of α that has worked well in practice is the peak of the spectrum signal power multiplied by the minimum of the spectrum signal power divided by 2*sub-array size. This is close to the value of α determined by eigendecomposition. It is easy to show that this value also has the correct units for α. Once α is chosen we use **PR** to estimate the resolution enhanced angular spectrum. The improvement in angular resolution and weak signal detection is evident.

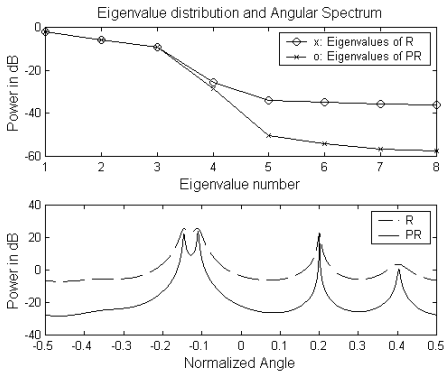

Fig. 4. Eigenspectrum and resolution comparison for spatial smoothing only and spatial smoothing plus **ASSP**. The two peaks near –0.1 are now clearly visible and the weak component ant 0.4 is at least 5 dB stronger. **ASSP** yields a higher apparent signal to noise ratio.

5. EXPERIMENTAL RESULTS

The prototype imaging system uses a wide beamwidth horn antenna for the transmitter that steps from 2-3 GHz in 40 steps at 5dBm. The center frequency is, F_c = 2.5 GHz or 12cm wavelength. The receiver consists of 12 vertically mounted discone antennas, spaced at $\lambda_c/2$ intervals. Discone properties include a dipole pattern, which is isotropic in azimuth, excellent bandwidth; the units constructed have a –20 dB return loss from 2-4 GHz. An important factor is their phase center, which remains constant over a wide frequency range. Figure 5 shows the array/receiver setup.

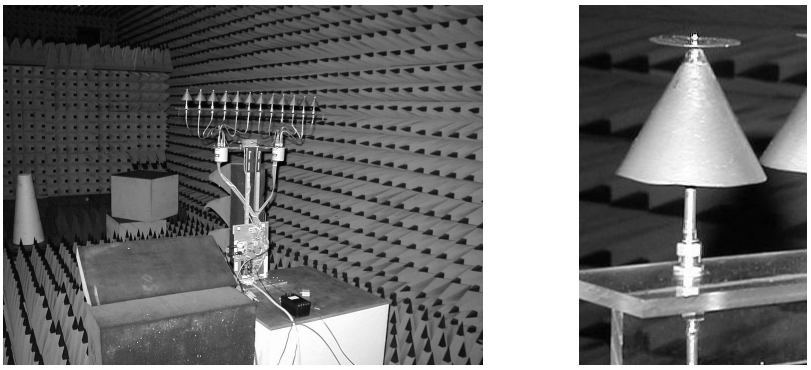

Fig. 5. Linear array imaging system in anechoic chamber. Operating frequency is 2-4 GHz. A discone element is on the right.

The targets consist of metal cylinders and dihedral reflectors. One particular case is 2 dihedrals placed 7 degrees apart at about 3.5 meters in range. The targets are sitting on a box near the back wall of the chamber. The dihedrals are approximately 75% of a beamwidth apart. The operating wavelength is about 12 cm therefore, if we go 10 wavelengths out, that is about 1.2 m away, which is just barely in the far field. However, correcting the steering vectors for near-field wave fronts did not improve image quality for ranges greater than 1.5 m., so the far field approximation is reasonable due to the small array size. The background clutter from the chamber is about 15 dB below the target returns. In Fig. 7 it is not possible to discern that there are 2 dihedrals, however in the Fig. 8 they are clearly visible. The region at about 3.5m and –20 to +20 degrees contains a row of large, rough but relatively flat objects with intermediate backscattering amplitude. Experimentally we have found that background clutter is diffuse in angle and degrades angular resolution. **ASSP** processing helps because the higher the threshold α, the more clutter is suppressed. This is most important when the number of elements is small, as in this case.

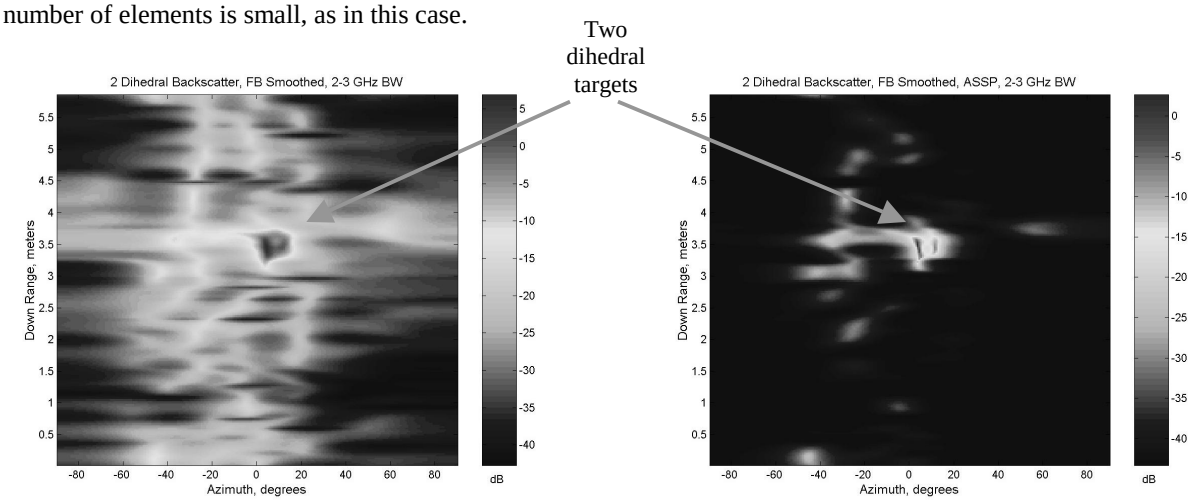

Fig. 7. Image of 2 dihedral reflectors, spatial smoothing only, and the same 2 dihedral reflectors processed with spatial smoothing and **ASSP** enhancement. The improvement in angular resolution is apparent as well as de-cluttering the background.

6. SOURCE LOCALIZATION IN NON-HOMOGENEOUS MEDIA

The imaging and beamforming results up to this point have assumed a homogenous, free space media for wave propagation. This implies a constant wave speed, which makes it easier to specify a model for the incident wave. In this section we will focus on the simplified case of changes in the refractive index of the propagating medium. We will assume that the material is lossless and non-dispersive, which removes frequency dependencies. We will also ignore any multiple scattering effects. If the environment contains deterministic boundaries where the index of refraction is constant or slowly varying, one should expect an unknown level of bias in any estimates of signal arrival angle. This is due to the fact that waves may be reflected or bent to follow paths that obscure the true source line-of-sight (LOS) angle. However in many cases the array still provides some estimate of the approximate LOS angle.

The phase of the incident fields at each antenna element can be estimated from the total path length from the source. The paths that the rays follow will be a function of the index of refraction along the way. Eventually, some rays will reach the antenna and form a phase front in that region. We have simulated deterministic as well as random refractive indices. The deterministic case follows as a simple case of random media that does not require the synthesis of statistical properties of the media. Deterministic indices of refraction can be used to investigate layers of material, walls in buildings or other known environments and boundaries. The equation $\Psi(\mathbf{k},\mathbf{r}) = \exp\left(j\mathbf{k}^H\mathbf{r}\right)$ describes the phase at each element from the projection of the known field onto the element positions. The wave vector **k** contains the angle of arrival information about the incident field near the antenna element. In this work we have used ray tracing to find the path length from source to each array element to estimate the phase at each element. The implementation of ray tracing is based on [17].

In this section we review the synthesis of two-dimensional non-homogenous media with precisely defined statistical characteristics. This section is adapted from [18] and [19]. The power spectral density of the refractive index is related to the autocorrelation function by a Fourier transform, and describes the probability distribution of random fluctuations in refractive index frequency. The fluctuations in the refractive index will be controlled by three parameters. The first two are the correlation lengths l_x and l_y, and the third is N_o, which is the root-mean-square amplitude of the fluctuation. Once the media is synthesized we are then ready to place our synthetic targets in the plane of the media at some specified range and angle and then compute the incident fields at the antenna.

The random refractive index is described in terms of its deviation from a value of one. The probability density function of the refractive index describes the statistics between two points in space. We assume a stationary process in this case. The fluctuation distribution can be chosen from several different types, such as Gaussian, Laplacian, Rayleigh or some other type. In this work we are primarily interested in the Rayleigh distribution because it most closely models natural phenomenon.

A Rayleigh distributed random variable (RV), with parameter σ is derived from a non-linear transformation of two Gaussian distributed RV's : $X_{Rayleigh} = \sqrt{N(0,\sigma)^2 + N(0,\sigma)^2}$. The coherence length of the refractive index profile is given by l_x and l_y. The power spectral density function of refractive medium, $W\left(k_x, k_y\right)$, is related to the correlation function via a two-dimensional Fourier transform. For a Gaussian correlation function,

$$W(k_x, k_y) = \frac{l_x l_y N_0^2}{4\pi} \exp\left(-\frac{k_x^2 l_x^2}{4} - \frac{k_y^2 l_y^2}{4} \right) \tag{11}$$

The refractive index profile $z = f(x, y)$ is related to the 2-D DFT of the power spectrum by

$$f(x, y) = \frac{1}{L^2} \sum_{m=-\frac{N}{2}}^{\frac{N}{2}-1} \sum_{n=-\frac{N}{2}}^{\frac{N}{2}-1} F(K_{xm}, K_{yn}) \exp\left(jK_{xm}x + jK_{yn}y \right) \tag{12}$$

where

$$F(K_{xm}, K_{ym}) = 2\pi L \sqrt{W\left(K_{xm}, K_{yn}\right)} \sum_{m=-\frac{N}{2}}^{\frac{N}{2}-1} \sum_{n=-\frac{N}{2}}^{\frac{N}{2}-1} N_\sigma(x, y) \exp\left(-jK_{xm}x - jK_{yn}y \right) \tag{13}$$

$$K_{xm} = \frac{2\pi m}{L}, \quad K_{yn} = \frac{2\pi n}{L}$$

where $N_\sigma(x, y)$ is a normally distributed 2-D random field with RMS amplitude σ. L is the size of the random field in wavelengths. From this set of equations we see that we are computing the 2-D Fourier transform of a Gaussian RV, then multiplying this by the Fourier transform of the correlation function, then inverse transforming to get the final 2-D field with the desired correlation properties.

Once the refracting medium has been synthesized, the next step is to place the targets or sources in the medium at a particular location specified by range and angle relative to the antenna that is at zero range. The simulation starts by assuming a point source model (over a specified angle) for the rays leaving the target. The ray tracing procedure terminates for a particular ray when it reaches the boundary of the imaged region. The total field at each element is estimated by storing the length of each ray that terminates very near to an array element. In the image formation algorithm, as frequencies are stepped, each ray will contribute a term $A\exp\left\{ j\left(2\pi f_m / c\right) l_{rn} \right\}$, for ray length l_{rn} at element *n*, frequency *m* and ray *r*, where *r* goes from one to the total number of rays at each element, which is variable depending on the environment. This approach easily accommodates multipath fields from a single source or multiple sources (targets).

7. COMPUTER SIMULATIONS IN NON-HOMOGENEOUS MEDIA

Figures 8 through 11 are computer simulations that demonstrate the use of wideband, adaptive array imaging in various non-homogeneous environments. In all cases the array is 12 elements, bandwidth from 2-3 GHz, located at the bottom center of the display, (i.e. at range zero, angle zero). The array is only 6 wavelengths in length, consequently it can estimate the field over a limited spatial area. Ray tracing is used to create the incident fields for a given environment, at each antenna element. The beamforming algorithm is then used to create the range-angle plot on the right in each case. Figure 8 shows a point source embedded in a Rayleigh distributed medium of correlation lengths of 0.5 λ and index fluctuation strength of 0.02. In this case there is only minor scattering from source to antenna. The source range and angle are estimated correctly. Figure 9 is a demonstration of a field incident upon a highly fluctuating slab of dielectric material. In this case the index fluctuation was set to 0.2 or 10x higher than figure 8. In this case we are still able to localize the source to a small cluster surrounding the true location. Note here that most of the cluster is delayed with respect to the true range of 24 meters. This is due to wandering of the ray paths, which makes them longer.

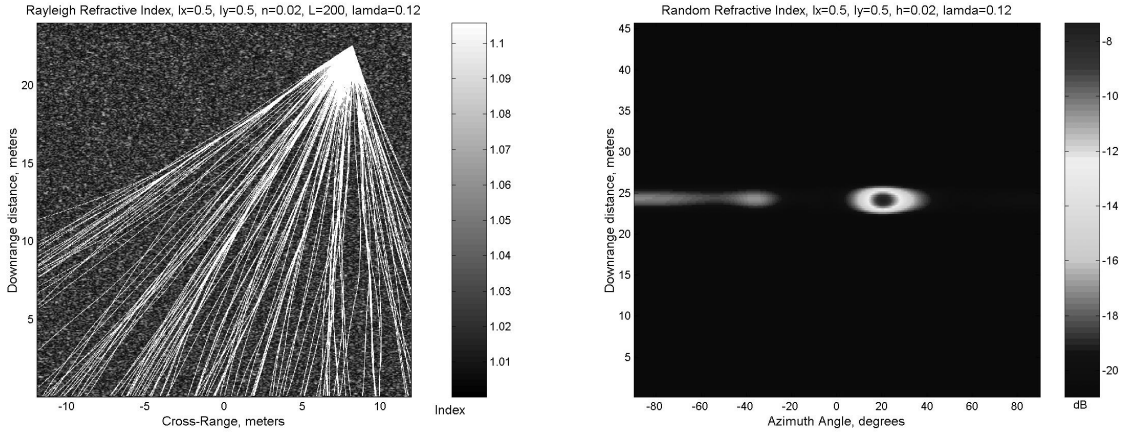

Fig. 8 Ray trace and range-angle plot for a single source embedded in a Rayleigh distributed medium. Source location is correctly estimated.

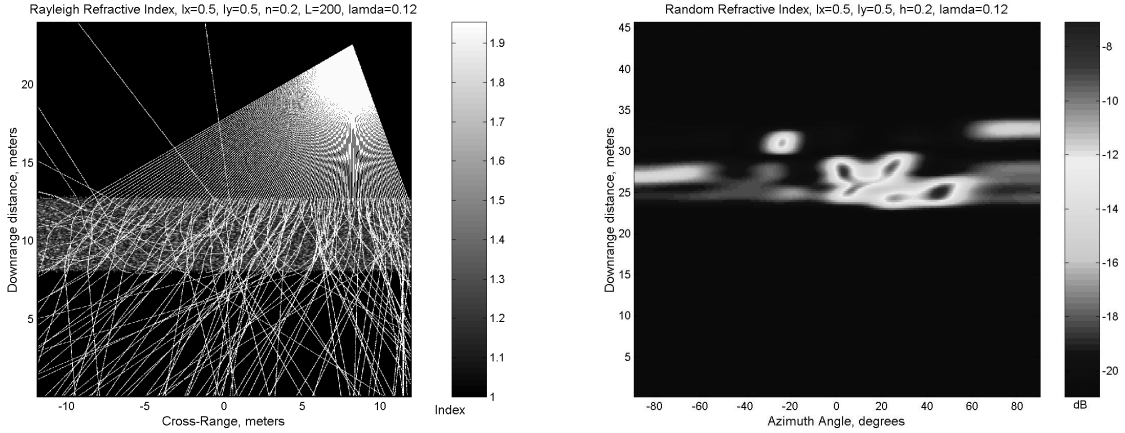

Fig. 9 Ray trace and range-angle plot for a single source incident upon a slab of Rayleigh distributed medium. In this case the index fluctuation is 10x higher than in Fig. 8. Source localization indicates multiple.targets in a compact cluster near the correct location plus some weaker outliers.

Figure 10 shows that a strong multipath component can be correctly estimated with this approach. The direct path at 24 meters and 20° is correctly estimated, as well as the image angle of -20°, but delayed due to the path differences. Figure 11 shows a model of an indoor environment, which is intended to show that an imaging algorithm can be biased due to the environment. In this case the strongest source has been estimated at about 40°, instead of the correct angle of 20° due to refraction by the walls and especially the joints in the walls. In this example we must be satisfied with simply being able to estimate the approximate the true LOS angle. Additionally, the total cluster is about evenly distributed around the true LOS angle.

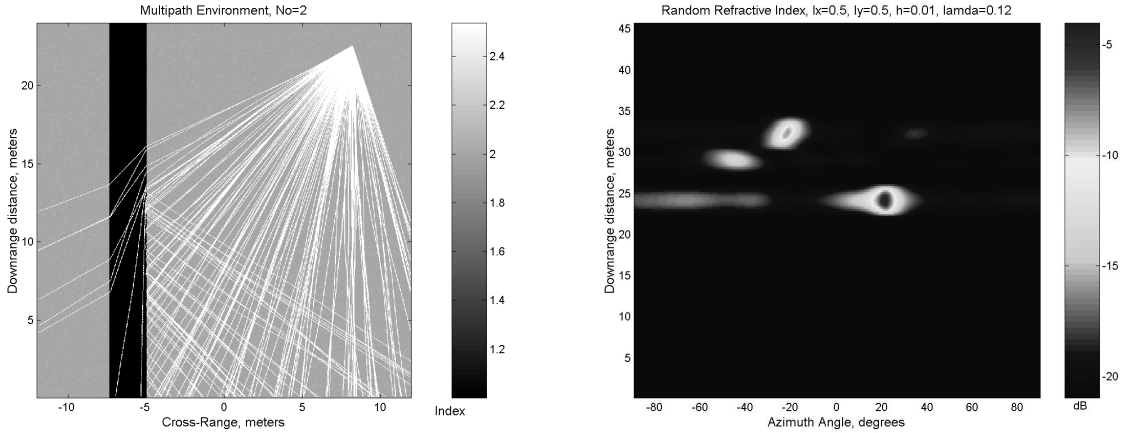

Fig. 10 This set of simulations shows the estimation of multipath signals in an environment with large regions of constant index of refraction.

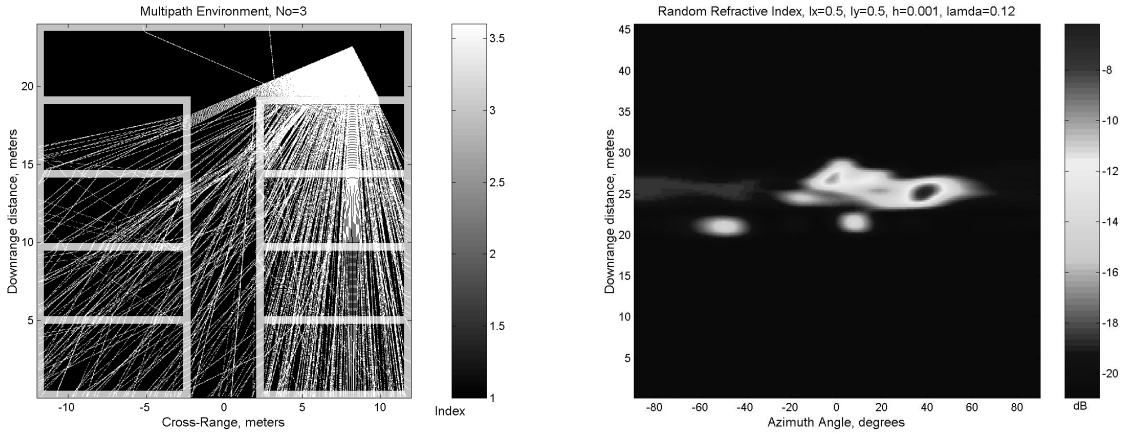

Fig. 11 This pair of images demonstrates that the estimation of the true LOS angle can be biased by the environment. Clearly as the medium gets more and more random, the ability to resolve the true LOS angle will diminish. The fields incident upon the array will become more and more diffuse, with less specular component.

Note that for rapidly fluctuating wave fronts, the incident signal phase at each element can vary rapidly with slight changes in position. This effect has been observed experimentally using a 4-element linear array for indoor angle of arrival measurements in real environments [3]. In the indoor environment the wave front distortion is primarily caused by scattering phenomenon that causes the superposition of many fields at the antenna, which leads to a non-planar field at the antenna. This leads to difficulty in determining the targets' true angle of arrival (AOA). We can expect some bias in the AOA estimate, with possible spurious peaks or eventually the target is not resolved and there will be only spurious responses. The effective rank of the signal covariance matrix will go up at each range bin, due to wave front

distortion because energy seems to come from many angles in the scattering environment. Consequently this will also cause problems with resolving multiple targets at the same range.

8. CONCLUSION

We have extended our previous work in free space, wide angle, wideband adaptive array imaging. In this work we have used ray tracing to simulate the incident fields upon a small, wideband adaptive array in non-homogeneous environments. We have demonstrated that after appropriate spatial resampling, and **ASSP** to reduce clutter, that the proposed adaptive beamforming approach can be used successfully in these types of environments that are likely to be encountered in practice. The motivation for this work is to provide high resolution, range-angle, microwave imagery for generally short range applications such as indoor personnel localization, missile seekers, or automotive radar.

REFERENCES

1. M. A. Curry and Y. Kuga, "*Radar Imaging Using a Wideband Adaptive Array*", Adaptive Sensor Array Processing Workshop, MIT Lincoln Laboratory, Lexington, Mass., March, 2000.
2. M. A. Curry and Y. Kuga, "*Radar Imaging Using a Wideband Adaptive Array*", IEEE 2000 International Radar Conf., Washington, DC, May, 2000.
3. M. A. Curry, M. Ciccotosto, B. Koala, Y. Kuga, "*Indoor Angle of Arrival Using Wide-band Frequency Diversity with Experimental Results and EM Propagation Modeling*", IEEE 2000 AP-S Conf. on Ant. and Prop. for Wireless Comm., Waltham, MA, Nov., 2000.
4. M. A. Curry, Y. Kuga, "*Experimental Results for Adaptive Radar Imaging in a Wide Angular Sector*", National Radio Science Meeting – URSI 2001, University of Colorado at Boulder, January, 2001
5. M. A. Curry, Kuga, Y., "*Experimental Results for Adaptive Radar Imaging in a Wide Angular Sector*", IEEE 2000 International Radar Conf., Atlanta, GA, May, 2001.
6. P. Grahn and S. Bjorklund, "*Short Range Radar Measurements using an Experimental Digital Array Antenna*", IEEE 2000 International Radar Conf., Washington, DC, May, 2000.
7. S. DeGraaf, "*SAR Imaging via Modern 2-D Spectral Estimation Methods*", IEEE Trans. on Image Processing", vol.7, pp. 729-761, 1998.
8. R. L. Fante, "*Adaptive Nulling of Sidelobe Discretes*", IEEE Trans. Aero. and Elec. Systems, vol. 35, no. 4, pp. 1212-1218, Oct., 1999.
9. G. R. Benitz, "*High-Definition Vector Imaging*",Lincoln Laboratory Journal, vol. 10, no. 2, pp. 147-170, 1997.
10. S. L. Borison, S. B. Bowling, and K. M. Cuomo, "*Super-Resolution Methods for Wideband Radar*," Lincoln Laboratory Journal, vol. 5, no. 3, pp. 441-462, 1992.
11. J. Krolik and D. Swingler, "*Focused Wide-Band Array Processing by Spatial Resampling*", IEEE Trans. Acoust., Speech, Signal Processing, vol. 38, No. 2, pp. 356-360, 1990.
12. J. Capon, "*High_Resolution Frequency-Wavenumber Spectrum Analysis*," Proc. IEEE, vol. 57, no. 8, pp. 1408-1419, 1969.
13. N. Wiener, "*Extrapolation, Interpolation and Smoothing of Stationary Time Series*", MIT Press, Cambridge, MA. 1949.
14. T. J. Shan, A. Paulraj and T. Kailath, "*On Spatial Smoothing for direction of arrival estimation of coherent signals*, " IEEE Trans. Acoust., Speech, Signal Processing, vol. ASSP-33, pp. 806-811, 1985.
15. K. J. Raghunath and U. V. Reddy, "*Finite data performance analysis of MVDR beamformer with and without spatial smoothing*", IEEE Trans. Acoust., Speech, Signal Processing, vol. 40, pp.2726-2736,1992.
16. J. Li, "*Improved Angular Resolution for Spatial Smoothing Techniques*", IEEE Trans. on Signal Processing, vol. 40, no. 12, 1992.
17. D. H. Johnson and D. E. Dudgeon, "*Array Signal Processing, Concepts and Techniques*", (Prentiss Hall), 1993.
18. P. Phu, "*MMW Experiments and Numerical Studies on the Enhanced Backscattering from Characterized Very Rough Surfaces*", Ph.D. Thesis, University of Washington, 1993.

19. M. A. Curry, "*Techniques for Radar Imaging using a Wideband Adaptive Array*", Ph.D. Thesis, University of Washington, 2001.

*curryma@gte.net; mark.a.curry@boeing.com; phone 1-425-697-2427, 5104 194th St. SW, Lynnwood, WA 98036;
**ykuga@u.washington.edu; Box 352500, Seattle, WA 98195-2500